RSC Advances

PAPER

View Article Online
View Journal | View Issue

Cite this: *RSC Adv.*, 2019, **9**, 14592

Copper–cobalt catalysts supported on mechanically mixed HZSM-5 and γ-Al_2O_3 for higher alcohols synthesis *via* carbon monoxide hydrogenation

Xuan Ge,[a] Hang Sun,[a] Kun Dong,[a] Yanqi Tao,[a] Qi Wang,*[a] Yazhong Chen,*[a] Genlei Zhang,[a] Peng Cui,[a] Ye Wang[b] and Qinghong Zhang[b]

Received 13th March 2019
Accepted 3rd May 2019

DOI: 10.1039/c9ra01927h

rsc.li/rsc-advances

Mechanically mixed γ-Al_2O_3 and HZSM-5 (Si/Al = 50) with different mass ratio were utilized as support for Cu–Co higher alcohol synthesis catalysts prepared through incipient wetness impregnation. The textural and structural properties were studied using Ar low temperature adsorption and desorption, H_2-temperature programmed reduction (H_2-TPR), X-ray diffraction (XRD), X-ray photoelectron spectroscopy (XPS), transmission electron microscope (TEM) and catalytic performance measurements. The results indicated that the mechanically mixed HZSM-5 and γ-Al_2O_3 supported copper–cobalt catalysts were superior to either γ-Al_2O_3 or HZSM-5 supported ones with the same metal loading. The results revealed that using HZSM-5 and γ-Al_2O_3 mechanically mixed benefited the dispersion of metallic phases and stronger synergetic functions between smaller nanoparticles containing copper and/or cobalt, which is essential for HAS from CO hydrogenation. Under working conditions of P = 5.0 MPa, T = 300 °C, $V(H_2) : V(CO) : V(N_2) = 4 : 2 : 1$ and GHSV = 7200 mL g^{-1} h^{-1}, mechanically mixed HZSM-5 and γ-Al_2O_3 supported catalysts showed higher catalytic activity than those over single support. For CuCo catalysts upon support containing 50.0 wt% HZSM-5 and 50.0 wt% γ-Al_2O_3, the CO conversion was 21.3% and the C_{2+} alcohol selectivity was 41.8%.

1 Introduction

Catalytic conversion of syngas to long-chain hydrocarbons and alcohols is one of the most attractive subjects in C_1 chemistry.[1–3] The hydrocarbons and alcohols obtained through the process could be used as fuels, fuel additives for octane value enhancement of gasoline or cetane value enhancement of diesel. Also intermediates for various value-added chemicals such as medicine, cosmetics and polyester. The most important aspect for carbon monoxide hydrogenation is the efficient tuning selectivity of various products through catalysts and the working conditions. Cobalt-based catalysts are efficient for the synthesis of long-chain paraffins using the famous Fischer–Tropsch process,[4] while copper-based catalysts are industrialized for large scale methanol synthesis from syngas. Nowadays, efficient catalysts for syngas conversion to mixed higher alcohols include Rh-based catalysts,[5] Cu–Co bimetallic catalysts[6–9] and molybdenum based catalysts.[10,11] Among the non-precious catalysts, Cu–Co bimetallic catalysts showed better selectivity of products and stability, attracting wide attention recently. Copper can activate CO non-dissociatively and subsequently generate alcohols, while cobalt enables the dissociative CO adsorption and C–C chain growth.[1,2] Generally, supports for Cu–Co catalysts include γ-Al_2O_3, SiO_2, ZrO_2, TiO_2, SBA-15 and ZSM-5.[9,12–16] Among them, γ-Al_2O_3 support was widely probed. The problems associated with the Cu–Co/γ-Al_2O_3 catalysts such as low CO conversion, poor selectivity and low dispersion of active species, were found. Jovana *et al.*[17] recently discovered that mixed Y-zeolite and γ-Al_2O_3 support could be combined through extrusion, and then Pt metal was separately loaded upon Y-zeolite or γ-Al_2O_3. Thus, the nanoscale distance between the acid sites and metal nanoparticle could be efficiently tuned for hydrocarbon conversion. López-Mendoza also found that hydrodesulphurization Co–Mo–W sulfide catalysts supported upon SBA-15 and SBA-16 mechanically mixed showed better performance than catalysts using either SBA-15 or SBA-16 as support.[18] They contributed the better performance to the bimodal pore structure formation, which favored the diffusion of catalyst precursors on the support and better dispersion of the active phases. Li *et al.*[19] utilized two types of SiO_2 with different mesopore size and HZSM-5 zeolite to prepare hybrid supported cobalt-based catalysts for Fischer–Tropsch synthesis. The hybrid supported catalysts showed higher performance and it was believed that mesopores provided quick mass transfer

[a]*Anhui Province Key Laboratory of Advanced Catalytic Materials and Reaction Engineering, School of Chemistry and Chemical Engineering, Hefei University of Technology, Hefei 230009, China. E-mail: wangqi@hfut.edu.cn; chenyazhong@hfut.edu.cn; Fax: +86-551-62901450; Tel: +86-551-62901450*

[b]*State Key Laboratory of Physical Chemistry of Solid Surface, College of Chemistry and Chemical Engineering, Xiamen University, Xiamen 361005, China*

channels, while the micropores contributed to high metal dispersion and accelerated hydrocracking/hydroisomerization reaction rate. Generally, using dual supports with different pore structure could significantly alter the dispersion of active species during catalyst preparation and diffusion of reagents, reaction pathways or intermediates for complex reactions such as higher alcohol synthesis (HAS) and Fischer–Tropsch synthesis.[20] Thus, in this work, we prepared copper–cobalt catalysts supported upon mechanically mixed γ-Al_2O_3 and HZSM-5 with different mass ratio to probe the pore structure evolution and their influences upon catalytic performance of HAS from CO hydrogenation.

2 Experimental

2.1 Catalyst preparation

The γ-Al_2O_3 was supplied by Liaoning Haitai Technology Incorporation. HZSM-5 (Si/Al = 50) powder (Nanjing University Catalyst Factory) were mixed together according to the desired mass ratio, then put into a planetary ball mill QM-3SP04 (Nanjing University Instrument Plant) at a certain rate of ball milling for 4.0 h. Thus, obtained powders were pressed into disks and then crushed, sieved to collect the grains of 60–80 mesh in size. The supports were described as Z_aA_b according to the mass ratio of HZSM-5 and γ-Al_2O_3 (a : b). For comparison, According to the above experimental steps, γ-Al_2O_3, HZSM-5 support with grain size of 60–80 mesh was also prepared. HZSM-5 + γ-Al_2O_3 support was described as a simple physical mixing of HZSM-5 and γ-Al_2O_3 after ball milling with a mass ratio of 1 : 1, and then obtained powders were pressed into disks and then crushed, sieved to collect the grains of 60–80 mesh in size. The copper–cobalt catalysts for HAS were prepared through incipient wetness impregnation process. The total metal nitrate loading was kept at 15.0 wt%, while the Cu/Co molar ratio was kept at 0.4. Typically, a certain amount of $Co(NO_3)_2 \cdot 6H_2O$ and $Cu(NO_3)_2 \cdot 3H_2O$ of analytical grade, purchased from Sinopharm Chemical Reagent Co., Ltd. and used without further purification, were weighed with an electronic balance, dissolving in a certain deionized water, then as prepared support such as Z_aA_b, HZSM-5 + γ-Al_2O_3, γ-Al_2O_3 and HZSM-5 were put into the solution for 24.0 h at ambient temperature. Then, the samples were dried at 100 °C for 6.0 h. After drying, the samples were put into a muffle furnace for calcination with a temperature ramp rate of 2 °C min^{-1} from 100 °C to 500 °C and kept for 5.0 h.

2.2 Catalyst characterizations

The specific surface areas of catalysts were determined through Ar adsorption at using Micromeritics ASAP 2020 M. Prior to adsorption, the samples were degassed at 80 °C for 2.0 h to remove physically adsorbed components under vacuum. The surface area was determined from the linear portion (P/P_0 = 0.05–0.30) of the Brunauer–Emmett–Teller (BET) equation. The mesopore volume and pore size distribution were calculated using the BJH model, while the micropore volume and pore size distribution were calculated using HK model. The pore diameter distribution was calculated by the BJH method using the adsorption branch of the isotherms.

X-ray powder diffraction (XRD) was used to determine the phase composition and particle size of the catalysts before and after reduction. The XRD measurements were performed on a Rigaku D/MAX2500VL/PC using nickel filtered Cu-Kα radiation (λ = 0.1541 nm), operating voltage of 40 kV and current of 40 mA. The intensity was measured by step scanning in the 2θ range between 10° and 90°, with a 2θ step of 0.02°. The average crystallite sizes were calculated using the peak width at half peak height and the Debye–Scherrer equation after background subtracting and correction for instrumental broadening.

Transmission microscopy microscope images were obtained using a JEM-2100F operated at 200 kV. TEM samples were prepared by the ultrasonic dispersion of slightly ground catalyst samples in ethanol for 30 min, and then a drop of the suspension was applied onto a holey carbon grid. The particle size distribution was calculated on monolayer particles by using SigmaScan software.

Temperature programmed reduction in H_2 (H_2-TPR) experiments were conducted on a self-made microreactor-gas chromatograph (GC) system using a 5% H_2–95% Ar atmosphere. The sample (20.0 mg) was heated from room temperature to 100 °C under 30.0 mL min^{-1} Ar flow and kept at 100 °C for at least 30 min, and then cooled down to room temperature. Then Ar was switched to 30.0 mL min^{-1} 5% H_2–95% Ar gas, and the sample was heated with a linear temperature rise from 50 °C to 700 °C at 10 °C min^{-1}. H_2 consumption was measured online with a thermal conductivity detector (TCD).

The surface species of the catalysts were detected using X-ray induced Auger electron spectroscopy (ESCALAB250Xi, Thermo Fisher). The spectrum was recorded with Al-Kα_1 as the exciting source ($h\lambda$ = 1486.6 eV). The binding energy or kinetic energy values for the Auger electron were calibrated using the C 1s peak of 284.7 eV as the reference.

2.3 Catalytic performance

The catalytic performance of each catalyst was evaluated using a stainless-steel tubular reactor. 5.0 mL catalyst was charged into the reactor. Then, the catalyst was activated in a hydrogen flux with a GHSV of 3000 h^{-1} at 400 °C for 12.0 h with a temperature ramp rate of 10 °C min^{-1} from ambient temperature. Then the temperature was lowered to 300 °C, a feeding gas mixture with a composition of $N_2 : H_2 : CO$ = 4 : 2 : 1 was delivered to reactor with a total GHSV of 7200 h^{-1}. The reaction pressure was maintained at 5.0 MPa through a backpressure regulator. The products were online monitored through a gas chromatograph (GC-2000 III) equipped with TCD and FID detectors. N_2, CO, CH_4, CO_2 in products were separated with 2.0 m TDX-01 carbon molecular sieve column using hydrogen as carrier gas and detected by TCD. Hydrocarbons and alcohols were separated with 15.0 m × 25 μm × 0.25 μm KB-Plot Q capillary column using N_2 as carrier gas and detected by FID. Conversion of CO was calculated using N_2 as internal standard according to the TCD analysis results. The selectivity to hydrocarbons and alcohols and their space time yields were calculated using carbon normalization method. Data with carbon balance and oxygen balance over 95% were utilized.

3 Results and discussion

3.1 Physiochemical properties

The texture properties of HZSM-5, Z_1A_1, HZSM-5 + γ-Al_2O_3 and γ-Al_2O_3 supports including BET surface areas, micropore volume, mesopore volume and micropore surface areas were displayed in Table 1 and Fig. 1. HZSM-5 support showed higher specific surface area and abundant micropore structure, while γ-Al_2O_3 support showed lower specific surface area and only mesopore structure. Supports on Z_1A_1 and HZSM-5 + γ-Al_2O_3 showed the specific areas between those of HZSM-5 and γ-Al_2O_3. For Z_1A_1 and HZSM-5 + γ-Al_2O_3 supports, the micropore surface areas, micropore volumes and mesopore volumes all showed only a physical mixture of separate phase, ball milling and simple physical mixing did not change the texture of each phase. Thus, the texture properties are combinations of each phase according to the mass ratio. The experimentally determined values are very close to the calculated ones. Fig. 1 showed the pore size distribution of mechanically mixed HZSM-5 and γ-Al_2O_3 using H–K or BJH models. In Fig. 1a, the HK model revealed that HZSM-5 showed very typical micropore structure of 0.5 nm, while γ-Al_2O_3 did not show micropore structure. For example, Z_1A_1 showed most probable pore size of 6.0 nm. HZSM-5 showed most probable pore size of 4.7 nm with small pore volume, suggesting the formation of secondary pore due to the packing of nanoparticles of HZSM-5 generated from ball milling and $CuCo/Z_aA_b$ is almost 70–80% respect to the original support surface area, which is indicative of the high dispersion of the active phases on the support and the possible formation of clusters of oxides of transition metals which occlude smaller pores.

Fig. 2 showed the high resolution TEM images of copper–cobalt catalysts supported on various carriers after reduction and passivation. The particle size distribution was also presented. From the results, it could be seen that the particle size of copper–cobalt bimetal possessed narrower distribution and smaller average particle sizes supported on HZSM-5 and γ-Al_2O_3 mechanically mixed than those supported either on HZSM-5 or on γ-Al_2O_3. The existence states of copper, cobalt species after reduction were found very complex, including forms such as metallic $Cu^{\delta+}$ (δ = 0–1) and Co^0, Cu–Co alloy,[8] core–shell structures such as Cu@Co or Co@Cu, and mixed nanoparticles.[15] At the same time, complete reduction of copper and cobalt species was hardly realized. Thus, a fraction of Cu^+ and Cu^{2+} also existed. Likewise, part of Co^{2+} also existed in the reduced catalysts, as revealed by XPS characterization in this work. The average particle size was estimated to be 2.87 nm for γ-Al_2O_3 supported catalyst and 2.78 nm for HZSM-5 supported catalyst (Fig. 2A). While for the mixed support, the average particle size decreased to 1.76 nm for catalyst supported on Z_1A_1. We ascribed the phenomenon to the fact that due to the mesopore modification by nanosized HZSM-5 during ball milling. As the pore size of HZSM-5 was only 0.5 nm, diffusion of catalyst precursor into the pore structure of HZSM-5 is difficult. Thus, only a small fraction of copper and cobalt species existed in the pore structure of HZSM-5, while a large fraction of copper and cobalt species existed outside the pore structure of HZSM-5. While for γ-Al_2O_3 supported copper–cobalt catalyst, the relative larger average pore size and wider distribution of pore size makes the nano-confinement effect smaller than those on mixed support with smaller average pore size and narrower

Table 1 The texture properties of various carriers

	BET ($m^2\ g^{-1}$)		Micropore area ($m^2\ g^{-1}$)		Micropore volume ($cm^3\ g^{-1}$)		Mesopore volume ($cm^3\ g^{-1}$)	
Sample	Support	Catalyst	Support	Catalyst	Support	Catalyst	Support	Catalyst
HZSM-5	392.3	271.0	265.6	254.0	0.125	0.11	—	—
Z_1A_1	296.4	217.7	149.0	132.4	0.103	0.060	0.37	0.16
γ-Al_2O_3	292.6	161.9	—	—	—	—	0.74	0.41
HZSM-5 + γ-Al_2O_3	342.1	229.5	160.2	146.5	0.134	0.083	0.43	0.23

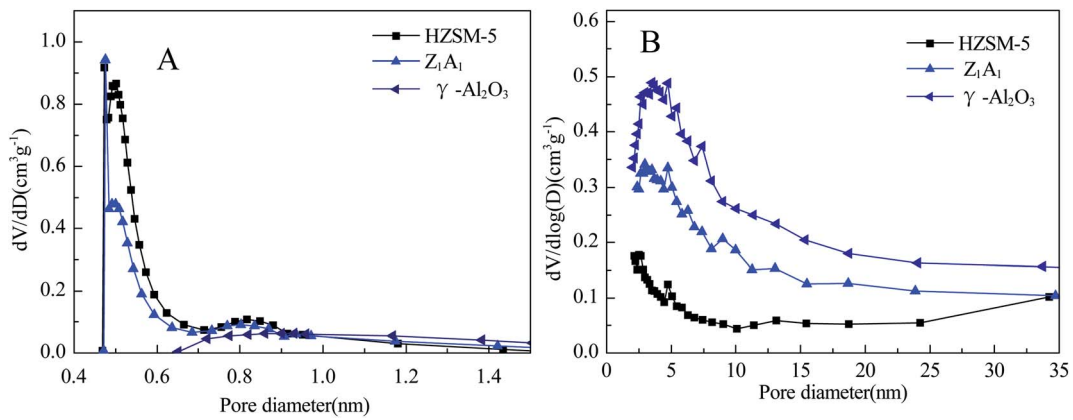

Fig. 1 The pore size distribution of supports: (A) HK model (B) BJH model.

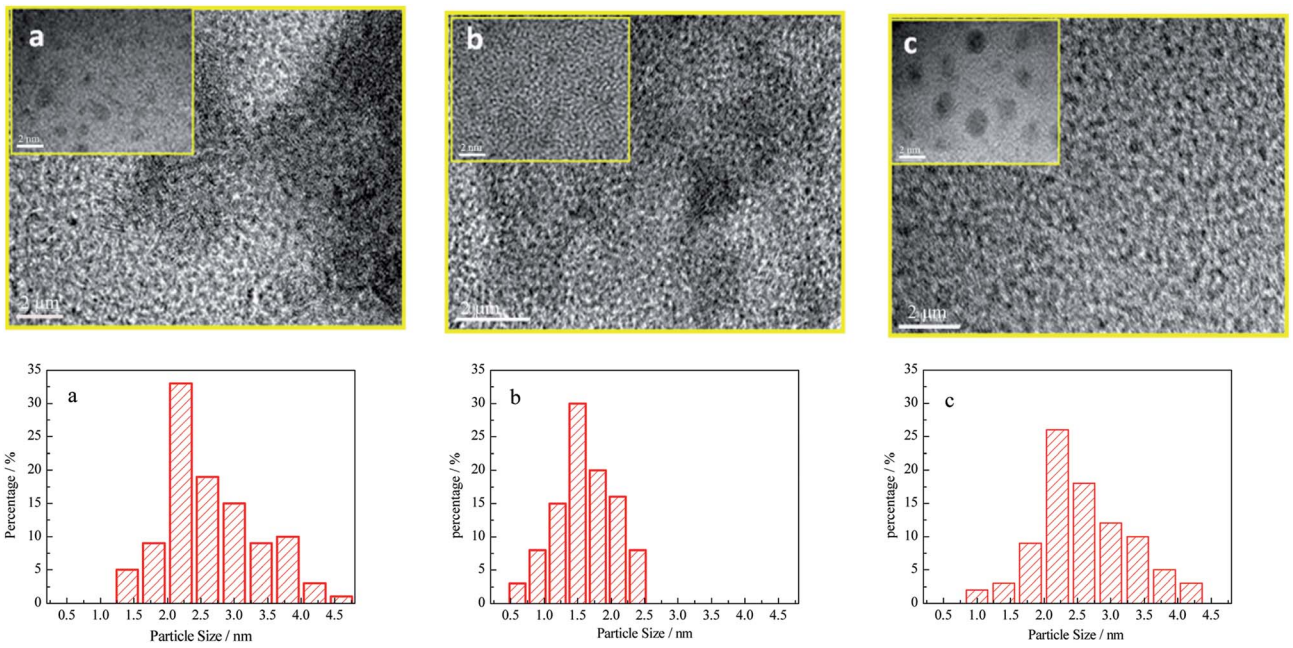

Fig. 2 TEM images of different catalysts and their particle size distribution ((a) Cu–Co/HZSM-5; (b) Cu–Co/Z_1A_1; (c) Cu–Co/γ-Al_2O_3).

pore size distribution.[21–24] According to the HAS mechanism over copper-modified Fischer–Tropsch synthesis catalyst, metallic Cu^0 absorbs CO associatively for the CO insertion reactions to form alcohols, while metallic Co^0 absorbs CO dissociatively to increase the carbon chains.[24] The close interaction between copper and cobalt species, are essential for structure sensitivity HAS reactions.

Fig. 3 and 4 presented the XPS spectra of Cu_{2p} and Co_{2p} in reduced catalysts. The binding energies, peak areas and specific ratio of surface species were listed in Tables 2 and 3. The Cu_{2p} spectrum, after peak splitting, identification and deconvolution analysis, suggested the presence of $Cu^{\delta+}$ (δ = 0–1) and Cu^{2+}, which corresponded to the binding energy of 932.5 eV and 933.5 eV, respectively. The $Cu^{\delta+}/Cu^{2+}$ specific ratios over HZSM-5, Z_1A_1 and γ-Al_2O_3 supported catalysts were 1.39, 1.59 and 1.41 respectively. Mixed support benefited the reduction of surface Cu^{2+} into $Cu^{\delta+}$. The Co_{2p} XPS spectrum suggested the presence of Co^0 and Co^{2+} in the reduced catalysts,[5] which corresponded to the binding energy of 778.3 eV and 780.2 eV, respectively. The specific ratio of Co^0/Co^{2+} ratios over HZSM-5, Z_1A_1 and γ-Al_2O_3 were 1.48, 0.94 and 1.34. It seemed that using Z_1A_1 support benefited the reduction of copper oxide species while to some extent hindered the reduction of cobalt species into Co^0.

Fig. 5 showed H_2-TPR profiles of copper–cobalt catalysts on various supports. It was found that both copper and cobalt species could be reduced and their reduction could be interacted. Wang *et al.*[25] found that for 5Cu15Co supported on γ-Al_2O_3, composite oxides such as $CuCo_2O_4$ and $Cu_xCo_{3-x}O_4$ spinel with

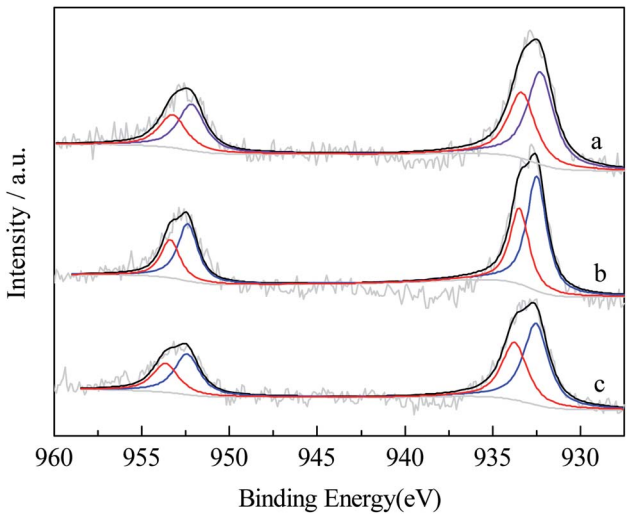

Fig. 3 XPS spectra of Cu 2p region for catalysts on various supports ((a) Cu–Co/HZSM-5; (b) Cu–Co/Z_1A_1; (c) Cu–Co/γ-Al_2O_3).

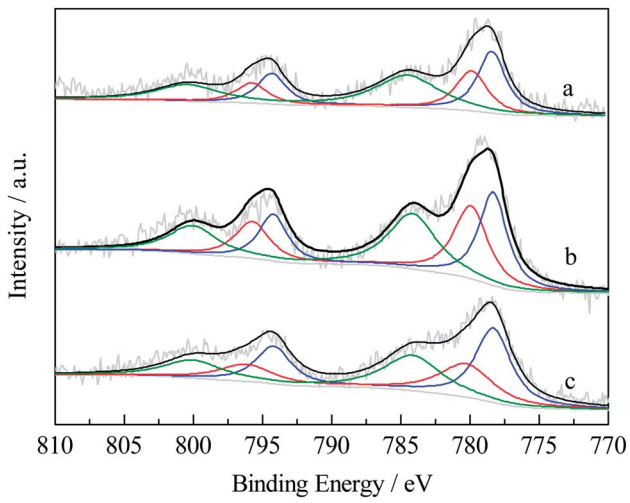

Fig. 4 XPS spectra of Co 2p region of catalysts on various supports ((a) Cu–Co/HZSM-5; (b) Cu–Co/Z_1A_1; (c) Cu–Co/γ-Al_2O_3).

Table 2 XPS data of Cu 2p region of catalysts on various supports

	Peak areas (AU)		
Position (eV)	Cu–Co/HZSM-5	Cu–Co/Z_1A_1	Cu–Co/γ-Al_2O_3
$Cu^{\delta+}$ (932.5 eV)	7628.9 (58.14%)	7029 (61.44%)	6328.6 (58.50%)
Cu^{2+} (933.5 eV)	5492.8 (41.86%)	4412 (38.56%)	4488.8 (41.50%)
$Cu^{\delta+}/Cu^{2+}$	1.39	1.59	1.41

high structure similarity with Co_3O_4 could be formed, thus the reduction temperature for cobalt species could be decreased. The peak temperature around 250 °C was ascribed to the reduction of CuO, while peak temperature around 290 °C was ascribed to the reduction of $CuCo_2O_4$. For Co_3O_4, peak reduction temperature was around 370 °C. In this work, the peak reduction temperature all shifted to higher ones than those reported by Wang due to the lower content of copper and cobalt species and nano-confinement effect of pore structure. For Cu–Co/HZSM-5 catalyst (Fig. 6a), two reduction peak temperatures, one at 300 °C and the other one at 420 °C, were observed. The 300 °C reduction peak corresponded to the reduction of CuO, while the 420 °C reduction peak temperature was attributed to the reduction of $CuCo_2O_4$. For Cu–Co/γ-Al_2O_3 catalyst (Fig. 5c), the peak temperature around 310 °C was ascribed to the reduction of CuO, the asymmetric reduction peak temperature overlapped in the range of 400–500 °C were ascribed to the reduction of $CuCo_2O_4$ and Co_3O_4. For the mixed supports (Fig. 5b), the hydrogen consumption peak temperatures became complex. The first peak reduction temperature appeared at 350 °C, the reduction of CuO became more difficult in comparison with both HZSM-5 and γ-Al_2O_3 supported catalysts. For the HZSM-5 supported catalysts, copper and cobalt species mainly existed on the outside of the surface although it showed larger surface area and micropore surface area due to its 0.5 nm pore size. Thus, the reduction temperature shifted to lower ones due to its smaller particle size and weaker interaction with the support. For the mixed supports, the peak reduction temperatures all shifted to lower ones, due to the smaller particle sizes of CuO and $CuCo_2O_4$ due to nano-confinement effect. The smaller of the pore size, the lower peak temperature for reduction were observed on CuCo catalysts on mixed supports. The modification of nano pore structure resulted in finer CuO and $CuCo_2O_4$ particles, showing different reduction behaviors.

Fig. 6 showed the XRD patterns of copper–cobalt catalysts supported on various supports in oxidation state. The results indicated that both copper species and cobalt species were highly dispersed, no XRD diffraction peaks was found for the copper or cobalt species, suggesting that CuO or Co_3O_4 particle size was

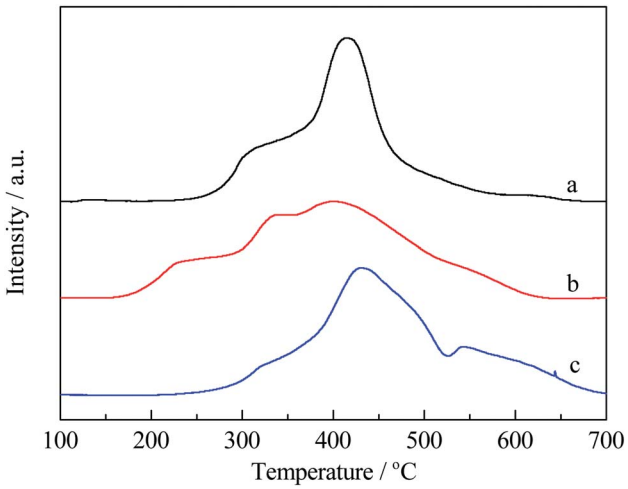

Fig. 5 H_2-TPR profiles for CuCo catalysts on different supports ((a) Cu–Co/HZSM-5; (b) Cu–Co/Z_1A_1; (c) Cu–Co/γ-Al_2O_3).

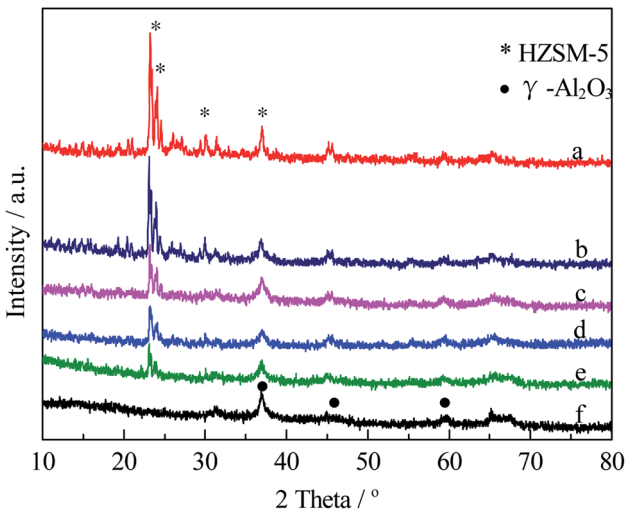

Fig. 6 XRD patterns for copper–cobalt catalysts supported over different supports ((a) Cu–Co/HZSM-5; (b) Cu–Co/$Z_1A_{0.5}$; (c) Cu–Co/Z_1A_1; (d) Cu–Co/Z_1A_2; (e) Cu–Co/Z_1A_4; (f) Cu–Co/γ-Al_2O_3).

very small or existed in an amorphous state.[19] XRD diffraction peaks for HZSM-5 with 2 theta values of 23.2°, 24.0° and 24.6° (Fig. 6a) or γ-Al_2O_3 with 2 theta values of 36.9°, 44.9° and 59.2° (Fig. 2f) were found. With the increase of γ-Al_2O_3 content in the support, the intensities for XRD peaks corresponding to HZSM-5 decreased, while those for γ-Al_2O_3 phase increased. No novel phase formation occurred during ball milling.

Table 3 XPS data of Co 2p region of catalysts on various supports

	Peak areas		
Position (eV)	Cu–Co/HZSM-5	Cu–Co/Z_1A_1	Cu–Co/γ-Al_2O_3
Co^0 (778.3 eV)	6031.90 (59.62%)	5706.48 (48.49%)	3849.10 (57.34%)
Co^{2+} (780.2 eV)	4085.78 (40.38%)	6062.03 (51.51%)	2864.01 (42.66%)
Co^0/Co^{2+}	1.48	0.94	1.34

Table 4 Catalytic performances of catalysts on various supports in terms of CO conversion and carbon-based selectivity of products[a]

Catalysts	CO conversion (%)	Selectivity products (C%)			
		Hydrocarbons	Methanol	C_{2-8} alcohols	CO_2
Cu–Co/HZSM-5	2.73	49.28	25.55	18.45	6.72
Cu–Co/$Z_1A_{0.5}$	20.15	41.71	17.98	33.87	6.44
Cu–Co/Z_1A_1	21.31	28.68	21.30	41.80	8.22
Cu–Co/Z_1A_2	18.16	35.11	18.87	38.13	7.89
Cu–Co/Z_1A_4	16.71	42.72	17.01	33.39	6.88
Cu–Co/γ-Al_2O_3	16.47	36.56	23.99	34.25	5.20
Cu–Co/HZSM-5+ Cu–Co/γ-Al_2O_3 (1 : 1)	9.42	41.82	21.40	30.35	6.43
Cu–Co/HZSM-5 + γ-Al_2O_3	17.78	35.24	22.34	35.45	6.97

[a] Working conditions: $T = 300$ °C, $P = 5.0$ MPa, GHSV = 7200 h^{-1}.

3.2 Catalytic performances

The catalytic performances in terms of CO conversion and selectivity to products were shown in Table 4. In order to investigate the effect of ball milling, catalyst containing 1 : 1 weight ratio of CuCo/HZSM-5 and CuCo/γ-Al_2O_3 were prepared and evaluated. The reaction products include C_1–C_8 straight alcohols and C_1–C_{10} normal paraffins and a small fraction of CO_2. The reaction products agreed with the Anderson–Schulz–Flory distribution. From Table 4, it could be seen that the catalytic performance of CuCo/HZSM-5 was unsatisfactory, conversion of CO was only 2.73%, and the selectivity to higher alcohols was only 18.45%. The catalytic performance of CuCo/γ-Al_2O_3 was better than CuCo/HZSM-5, with CO conversion of 16.47% and selectivity to higher alcohols of 43.25%. Interestingly, catalyst containing 1 : 1 weight ratio of CuCo/HZSM-5 and CuCo/γ-Al_2O_3 showed catalytic performance in terms of CO conversion and selectivity to higher alcohols just the same as the weighted mean performance of CuCo/HZSM-5 and CuCo/γ-Al_2O_3. No interaction between the two catalysts occurred. However, CuCo catalyst over mixed supports showed superior performance than both CuCo/HZSM-5 and CuCo/γ-Al_2O_3. Among them, CuCo/Z_1A_1 showed best performance under working conditions of $T = 300$ °C, $P = 5.0$ MPa and GHSV = 7200 h^{-1}. Conversion of CO reached 21.3% and selectivity to higher alcohols was 41.80%. The catalytic activity of CuCo/Z_1A_1 was higher than that of CuCo/HZSM-5 + γ-Al_2O_3, which indicated that the composite support of ball milling was more advantageous to the catalytic activity than the simple physical composite support. Further increase the γ-Al_2O_3 content in Z_aA_b supports resulted in poorer performance. The Ar physical adsorption results indicated that with the increase of γ-Al_2O_3 content in Z_aA_b supports, the ratios between the mesopore volumes and micropore volumes increased, from at the same time, the pore size also increased. The increased pore size favored the growth of metallic particles during reduction and reaction. Thus, poorer performance could be predicted, as revealed in Table 4. CuCo/γ-Al_2O_3 showed highest mesopore volume and largest most probable pore size, while its catalytic performance was poorer than the CuCo catalysts using Z_aA_b supports. The reasons were ascribed to the following factors. Firstly, ball milling of HZSM-5 and γ-Al_2O_3 resulted in smaller mesopore size of Z_aA_b supports, at the same time introduced a portion of micropore into the catalyst. Secondly, the smaller mesopore of support benefited the dispersion of copper and cobalt species due to the nano-confinement effect, thus, smaller mixed nanoparticles of core–shell structure or Cu–Co alloy essential for HAS could be obtained. Thirdly, mesopore is very important for reagents diffusion to active sites, while micropore were important to grantee the formation of normal paraffin and straight carbon chain alcohols. Proper micropore volume to mesopore volume ratio was found closely related with CO conversion and selectivity to higher alcohols.

4 Conclusions

Ball milling HZSM-5 and γ-Al_2O_3 mixture altered the pore structure of γ-Al_2O_3, retaining part of pore volume but decreasing the most probable pore size. CuCo bimetallic catalysts over the mixed supports showed smaller average particle size and better dispersion of cobalt and copper species, as evidenced by the TEM characterization. Due to the nano-confinement effects of nano pore, better performances were observed for CuCo catalysts over mixed supports. H_2-TPR results suggested copper and cobalt species in the smaller mesopores of supports were easier to reduction, increasing $Cu^{\delta+}/Cu^{2+}$ ratio while decreasing the Co^0/Co^{2+} ratio (a factor closely related with the carbon chain growth). Thus, higher CO conversion and selectivity to higher alcohols were obtained. Over CuCo/Z_1A_1 catalyst, CO conversion could reach 21.3% and selectivity to higher alcohols of 41.80%. Through the pore modification and nano confinement effects, smaller nanoparticles for copper and cobalt species with close interaction could be obtained, which were supposed to be very important for higher alcohols synthesis from CO hydrogenation.

Conflicts of interest

There are no conflicts to declare.

Acknowledgements

This work is financially supported by Open Project of State Key Laboratory of Physical Chemistry of Solid Surfaces (201412).

References

1 H. T. Luk, C. Mondelli, D. C. Ferré and J. A. Stewart, Status and prospects in higher alcohols synthesis from syngas, *Chem. Soc. Rev.*, 2016, **46**, 1358–1427.
2 W. Zhou, J. C. Kang and Y. Wang, Direct Conversion of Syngas into Methyl Acetate, Ethanol, and Ethylene by Relay Catalysis via the Intermediate Dimethyl Ether, *Angew. Chem., Int. Ed.*, 2018, **130**, 12188–12192.
3 Y. Xiang and N. Kruse, Cobalt–copper based catalysts for higher terminal alcohols synthesis via Fischer–Trops, *J. Energy Chem.*, 2016, **25**, 895–906.
4 Y. W. Lu, P. Zhou and F. Yu, Fischer–Tropsch synthesis of liquid hydrocarbons over mesoporous SBA-15 supported cobalt catalysts, *RSC Adv.*, 2015, **5**, 59792–59803.
5 V. Abdelsayed, D. Shekhawat, J. A. Poston Jr and J. J. Spivery, Synthesis, characterization, and catalytic activity of Rh-based lanthanum zirconate pyrochlores for higher alcohol synthesis, *Catal. Today*, 2013, **207**, 65–73.
6 J. Wang, P. A. Chernavskii and A. Khodakov, Structure and catalytic performance of alumina-supported copper-cobalt catalysts for carbon monoxide hydrogenation, *J. Catal.*, 2012, **286**, 51–61.
7 L. Wang, A. Cao, G. Liu, L. Zhang and Y. Liu, Bimetallic CuCo nanoparticles derived from hydrotalcite supported on carbon fibers for higher alcohols synthesis from syngas, *Appl. Surf. Sci.*, 2016, **360**, 77–85.
8 Y. Fang, Y. Liu, W. Deng and J. Liu, Cu-Co bi-metal catalyst prepared by perovskite $CuO/LaCoO_3$ used for higher alcohol synthesis from syngas, *J. Energy Chem.*, 2014, **23**, 527–534.
9 Y. Yang, X. Qi, X. Wang, D. Lv, F. Yu, L. Zhong, H. Wang and Y. Sun, Deactivation study of CuCo catalyst for higher alcohol synthesis via syngas, *Catal. Today*, 2016, **270**, 101–107.
10 L. Li, C. Hu and W. Liu, The origin of Mo promotion during H_2 pretreatment on an Fe catalyst for Fischer–Tropsch synthesis, *RSC Adv.*, 2017, **7**, 44474–44481.
11 M. K. Rohollah, N. Tahereh, T. Ahmad and K. Ali, Effect of elemental molar ratio on the synthesis of higher alcohols over Co-promoted alkali-modified Mo_2C catalysts supported on CNTs, *J. Energy Chem.*, 2015, **24**, 278–284.
12 V. R. Rao Pendyala, W. D. Shafer and G. Jacobs, Effects of Co/Ce molar ratio and operating temperature on nanocatalyst performance in the Fischer–Tropsch synthesis, *RSC Adv.*, 2017, **7**, 7793–7800.
13 Z. Wang and J. J. Spivey, Effect of ZrO_2, Al_2O_3 and La_2O_3 on cobalt–copper catalysts for higher alcohols synthesis, *Appl. Catal., A*, 2015, **507**, 75–81.
14 A. Y. Khodakov, V. L. Zholobenko and R. Bechara, Impact of aqueous impregnation on the long-range ordering and mesoporous structure of cobalt containing MCM-41 and SBA-15 materials, *Microporous Mesoporous Mater.*, 2005, **79**, 29–39.
15 Y. He, M. Liu, C. Dai, S. Xu, Y. Wei, Z. Liu and X. Guo, Modification of nanocrystalline HZSM-5 zeolite with tetrapropylammonium hydroxide and its catalytic performance in methanol to gasoline reaction, *Chin. J. Catal.*, 2013, **34**, 1148–1158.
16 G. Liu, T. Niu, D. Pan, F. Liu and Y. Liu, Preparation of bimetal Cu–Co nanoparticles supported on meso–macroporous SiO_2 and their application to higher alcohols synthesis from syngas, *Appl. Catal., A*, 2014, **483**, 10–18.
17 J. Zečević, G. Vanbutsele, K. P. Jong and J. A. Martens, Nanoscale intimacy in bifunctional catalysts for selective conversion of hydrocarbons, *Nature*, 2015, **528**, 245–248.
18 M. A. López-Mendoza, R. Nava, C. Peza-Ledesma, B. Millán-Malo, R. Huirache-Acuna, P. Skewes and E. M. Rivera-Munoz, Characterization and catalytic performance of Co-Mo-W sulfide catalysts supported on SBA-15 and SBA-16 mechanically mixed, *Catal. Today*, 2016, **271**, 114–126.
19 Y. P. Li, T. J. Wang and C. Z. Wu, Gasoline-Range Hydrocarbon Synthesis over Cobalt-Based Fischer–Tropsch Catalysts Supported on SiO_2/HZSM-5, *Energy Fuels*, 2008, **22**, 1897–1901.
20 K. Jothimurugesan and S. K. Gangwal, Titania-Supported Bimetallic Catalysts Combined with HZSM-5 for Fischer–Tropsch Synthesis, *Ind. Eng. Chem. Res.*, 1998, **37**, 1181–1188.
21 C. F. Wang, S. J. Guo, X. L. Pan, W. Chen and X. H. Bao, Tailored cutting of carbon nanotubes and controlled dispersion of metal nanoparticles inside their channels, *J. Mater. Chem.*, 2008, **18**, 5782–5786.
22 W. Chen, X. L. Pan and X. L. Bao, Tuning of Redox Properties of Iron and Iron Oxides via Encapsulation within Carbon Nanotubes, *J. Am. Chem. Soc.*, 2007, **129**, 7421–7426.
23 W. Chen, Z. L. Fan, X. L. Pan and X. H. Bao, Effect of Confinement in Carbon Nanotubes on the Activity of Fischer–Tropsch Iron Catalyst, *J. Am. Chem. Soc.*, 2008, **130**, 9414–9419.
24 X. L. Pan, Z. L. Fan, W. Chen, Y. J. Ding, H. Y. Luo and X. H. Bao, Enhanced ethanol production inside carbon-nanotube reactors containing catalytic particles, *Nat. Mater.*, 2007, **6**, 507–511.
25 J. Wang, X. Zhang, Q. Sun, S. Chan and H. Su, Chain growth mechanism on bimetallic surfaces for higher alcohol synthesis from syngas, *Catal. Commun.*, 2015, **61**, 57–61.